iScience

CellPress
OPEN ACCESS

Article

Sustained Adrenergic Activation of YAP1 Induces Anoikis Resistance in Cervical Cancer Cells

Yang Li, Shanshan Yang, Nouara C. Sadaoui, ..., Steve W. Cole, Susan K. Lutgendorf, Anil K. Sood

asood@mdanderson.org

HIGHLIGHTS

Daily restraint stress increases tumor growth and metastatic tumor burden

Norepinephrine protects cervical cancer cells from anoikis

Norepinephrine induces YAP1 dephosphorylation and nuclear translocation

Norepinephrine - induced anoikis resistance can be reversed by propranolol

Li et al., iScience *23*, 101289
July 24, 2020
https://doi.org/10.1016/j.isci.2020.101289

iScience

CellPress
OPEN ACCESS

Article

Sustained Adrenergic Activation of YAP1 Induces Anoikis Resistance in Cervical Cancer Cells

Yang Li,[1,2,10] Shanshan Yang,[3,10] Nouara C. Sadaoui,[1] Wei Hu,[1] Santosh K. Dasari,[1] Lingegowda S. Mangala,[1] Yunjie Sun,[1] Shuangtao Zhao,[4] Linghua Wang,[4] Yuan Liu,[1] Lois M. Ramondetta,[1] Ke Li,[5] Chong Lu,[5] Yu Kang,[5] Steve W. Cole,[6] Susan K. Lutgendorf,[7] and Anil K. Sood[1,8,9,11,*]

SUMMARY

Chronic stress-related hormones modulate tumor pathogenesis at multiple levels; however, the molecular pathways involved in stress and cervical cancer progression are not well understood. We established a preclinical orthotopic mouse model of cervical cancer and used the model to show that daily restraint stress increased tumor growth and metastatic tumor burden. Exposure to norepinephrine significantly protected cervical cancer cells from anoikis. We demonstrated that YAP1 was dephosphorylated and translocated from the cytoplasm to the nucleus by norepinephrine, a process initiated by ADRB2/cAMP/protein kinase A activation. Furthermore, anoikis resistance and YAP1 activation induced by norepinephrine could be rescued by a broad β-adrenergic receptor antagonist, propranolol. Collectively, our results provide a pivotal molecular pathway for disrupting pro-tumor neuroendocrine signaling in cervical cancer.

INTRODUCTION

A substantial number of studies have established an important role for biobehavioral stress factors in cancer progression (Antoni and Dhabhar, 2019; Lu et al., 2019; Umamaheswaran et al., 2018). Environmental and psychosocial processes initiate a cascade of signaling in both the central and peripheral nervous systems, which trigger fight-or-flight stress responses and release of stress-related mediators including catecholamines (norepinephrine [NE] and epinephrine), cortisol, and other neurotransmitters via the hypothalamic-pituitary-adrenocortical (HPA) axis or the sympathetic nervous system (SNS) (Antoni et al., 2006). Previously, we demonstrated that SNS activation can promote tumor metastasis-related pathways (Cole et al., 2015) in ovarian cancer. Although research has shown that stress hormones affect tumor pathogenesis at multiple levels, our understanding of the underlying mechanisms is in its infancy and needs to be expanded.

Cervical cancer is the fourth most common malignancy in women worldwide, with an estimated 570,000 new cases in 2018, representing 6.6% of all cancers in women (Bray et al., 2018). Human papillomavirus (HPV) infection is a well-recognized causative factor for cervical cancer (Burd, 2003). It has been reported that severely stressful life events were associated with a 62% increased risk of HPV16 infection, high viral load, and recurrent infection (Lu et al., 2016); psychologic distress had an increased risk of cervical cancer-specific mortality (Lu et al., 2019). Chronic stress is thought to suppress protective immunity that is critical for eliminating immunogenic cancers (e.g., squamous cell and basal cell carcinomas) and virally associated cancers (e.g., HPV-associated cervical, anal, and oral cancers) (Antoni and Dhabhar, 2019). At present, the molecular pathways by which chronic stress affects cervical cancer progression are not well understood.

In this study, we established a preclinical orthotopic mouse model of cervical cancer to determine the physiologic effects of chronic stress *in vivo* and identified YAP1 activation as a potential stress effector involved in anoikis resistance, which promotes cervical cancer progression.

RESULTS

Chronic Stress Promotes Cervical Cancer Growth *In Vivo*

Given the lack of established models of cervical cancer for assessing the effects of chronic stress, we sought to establish such a model. First, to identify cell lines that could be affected by stress hormones, we tested

[1]Department of Gynecologic Oncology and Reproductive Medicine, The University of Texas MD Anderson Cancer Center, Houston, TX, USA

[2]Department of Gynecologic Oncology, Women's Hospital, School of Medicine, Zhejiang University, Hangzhou, China

[3]Department of Gynecologic Radiotherapy, Harbin Medical University Cancer Hospital, Harbin, China

[4]Department of Genomic Medicine, The University of Texas MD Anderson Cancer Center, Houston, TX, USA

[5]Department of Obstetrics and Gynecology of Shanghai Medical School, Fudan University, Shanghai, China

[6]Cousins Center for Psychoneuroimmunology and Department of Psychiatry and Biobehavioral Sciences, Division of Hematology/Oncology, David Geffen School of Medicine, University of California, Los Angeles, CA, USA

[7]Department of Psychological & Brain Sciences, Division of Gynecologic Oncology, Department of Obstetrics & Gynecology, Department of Urology, Holden Comprehensive Cancer Center, University of Iowa, Iowa City, IA, USA

[8]Center for RNA Interference and Non-Coding RNAs, The University of Texas MD Anderson Cancer Center, Houston, TX, USA

[9]Department of Cancer Biology, The University of Texas MD Anderson Cancer Center, Houston, TX, USA

[10]These authors contributed equally

Continued

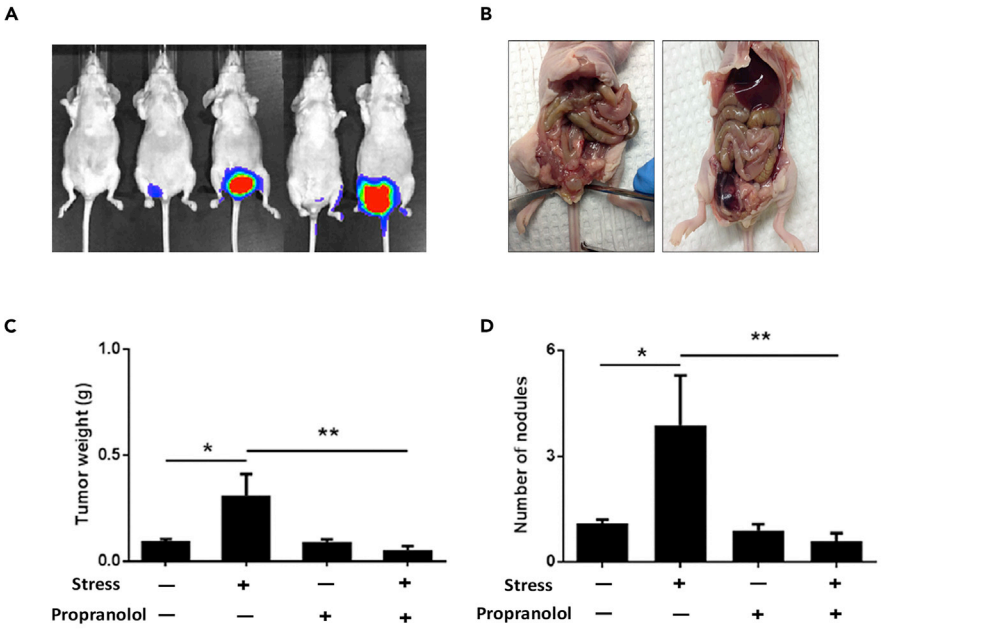

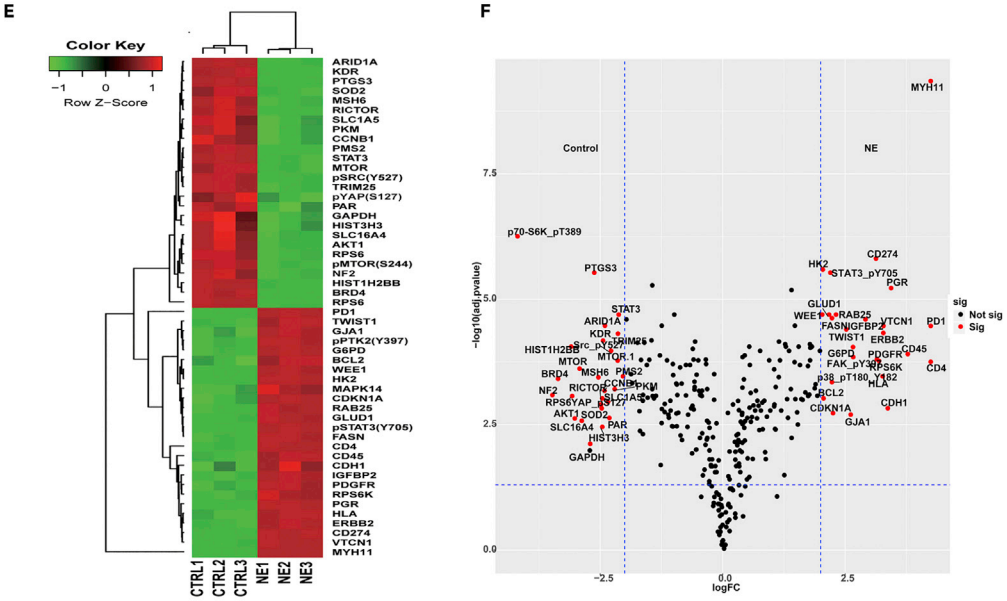

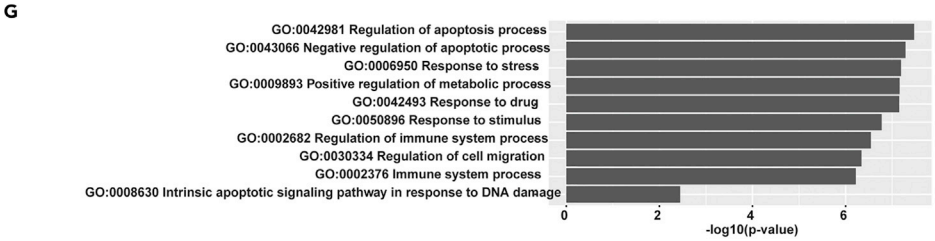

[11]Lead Contact

*Correspondence:
asood@mdanderson.org

https://doi.org/10.1016/j.isci.2020.101289

Figure 1. Stress Triggers Cervical Tumor Progression and Induces Specific Protein Expression Pattern in Cervical Cancer Cells

(A–D) (A) Representative images of tumor growth in nude mice over the course of 5 weeks obtained by a Xenogen *in vivo* imaging system (IVIS) and (B) established tumors in the mice at necropsy. Effects of restraint stress and propranolol (Prop) on (C) cervical tumor weight and (D) metastatic nodule formation. n = 10 per group.

(E and F) (E) Heatmap and (F) volcano plot of 52 differentially expressed proteins by reverse phase protein array (RPPA) analysis in SiHa cells treated with 10 μM NE for 12 h compared with no treatment.

(G) Gene Ontology analysis for functional enrichment. Data are presented as mean ± standard deviation (SD). The raw data for the RPPA are shown in Data S1. Differences between treatment groups were determined by orthogonal contrasts and denoted as follows: *$p < 0.05$, and **$p < 0.01$.

multiple cervical (SiHa, CaSki, ME-180, C33A) and ovarian (SKOV3 and A2780) cancer cell lines for β-adrenergic receptors. Most of these cell lines expressed varying levels of β-adrenergic receptors, but the C33A and A2780 cell lines lacked β2-adrenergic receptor (ADRB2) expression (Figure S1).

To evaluate the potential role of chronic stress on cervical cancer *in vivo*, a restraint-stress orthotopic model of cervical cancer was established and characterized. Cervical cancer cells were injected directly into the cervix at the cervical-uterine junction. We found that SiHa and ME-180, but not CaSki cells, had tumorigenic potential. Three days later, nude mice were placed in a movement-restricted space for 2 h daily to mimic chronic stress (Thaker et al., 2006). The mice were subjected to daily restraint stress for 3 weeks, then euthanized 1 week after stress was ceased. Tumor growth was monitored weekly by IVIS bioluminescence imaging for the duration of the experiment. Bioluminescence imaging showed tumor localization at the cervix within the pelvic region (Figure 1A). Further necropsy showed lymph-vascular invasion of tumors and spread into the parametrium and pelvic wall (Figure 1B). Representative hematoxylin and eosin (H&E) staining of the tumor tissues is shown in Figure S2. This model resembles the disease observed in the clinic; thus, it was adopted by our laboratory for further studies. Animals subjected to daily restraint stress had significantly greater tumor weight ($p < 0.05$) and higher metastatic tumor burden ($p < 0.05$) than non-stressed control mice that received the same injection of SiHa cells (Figures 1C and 1D). Of note, the broad β-antagonist propranolol inhibited stress-induced increases in both tumor weight ($p < 0.01$) and metastatic burden ($p < 0.01$).

NE Induces Anoikis Resistance Mediated by Decreased YAP1 Phosphorylation and NF2

To identify potential mechanisms of NE action during cervical cancer progression, we performed reverse phase protein array (RPPA) analysis in SiHa cells treated with or without 10 μM NE for 12 h. As shown in the heatmap (Figure 1E) and volcano plot (Figure 1F), there were 26 upregulated and 26 downregulated proteins in the NE-treated group.

Then, we performed Gene Ontology (GO) analysis for functional enrichment. Among the most prominent GO functions in the differentially expressed genes in the NE treatment group, regulation of apoptosis process was significantly enriched (Figure 1G). Apoptosis can be induced by numerous triggers, including the loss of cell anchorage, or anoikis. Resistance to anoikis is a hallmark of metastasis, affording tumor cells longer survival in the absence of matrix attachment and facilitating migration, reattachment, and colonization of secondary sites (Sood and Lutgendorf, 2011).

To validate whether NE could induce anoikis resistance, we cultured CaSki, ME-180, and C33A cervical cancer cells in ultra-low attachment plates, which allow for anchorage-independent growth. When treated with 10 μM NE for 72 h, CaSki ($p < 0.05$) and ME-180 ($p < 0.0001$) cells, which are ADRB2 positive, were significantly protected from anoikis, but the ADRB-negative C33A cells were not ($p > 0.05$) (Figure 2A). Similarly, SiHa, CaSki, and ME-180 cells had significantly greater migration and invasion when treated with NE, but C33A cells did not (Figure S3). Furthermore, immunohistochemical analysis of apoptosis in tumor sections revealed that cleaved caspase-3-positive cells in mice subjected to 21 days of daily restraint stress as described above were reduced compared with those among controls ($p < 0.01$; Figures 2B and 2C). These effects were attenuated in the group that was both stressed and treated with propranolol ($p < 0.01$; Figures 2B and 2C).

To uncover potential pathways involved in NE-induced anoikis in cervical cancer, additional computational analysis of differentially expressed genes using the Kyoto Encyclopedia of Genes and Genomes (KEGG) showed the top ten enriched pathways (Figure 2D): seven pathways in signal transduction, two in human

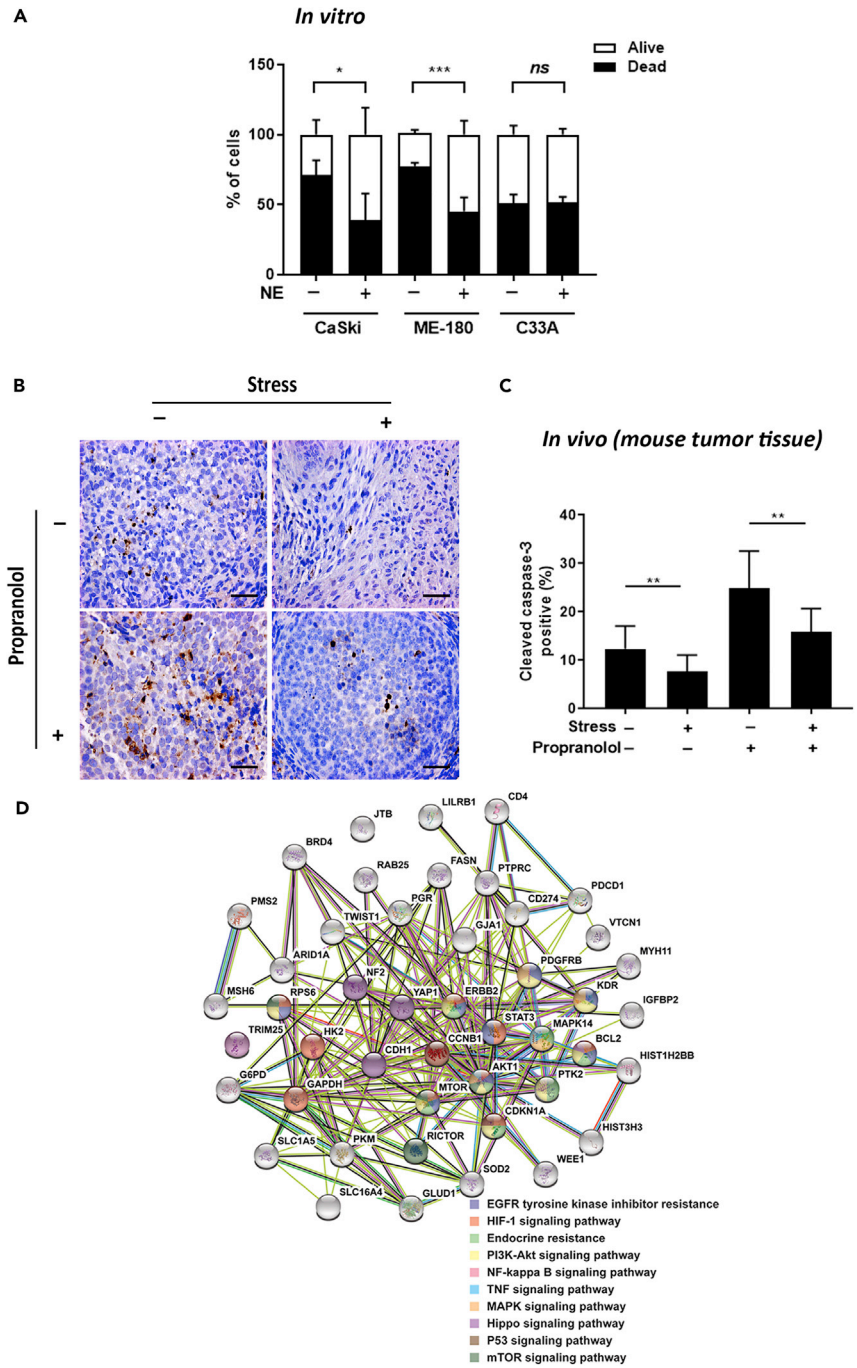

Figure 2. Norepinephrine (NE) Induces Anoikis Resistance and Putative Pathways in Cervical Cancer Cells

(A) Number of dead (SYTOX Red-positive, black) and living (SYTOX Red-negative, white) CaSki, ME-180, and C33A cells after 72 h of low attachment and/or co-incubation with 10 μM NE.

(B and C) (B) Representative immunohistochemistry and (C) quantification staining of apoptosis protein marker in mouse cervical tumors in various conditions. n = 6 mice per group. Scale bar is 200 μm.

(D) Kyoto Encyclopedia of Genes and Genomes (http://www.genome.ad.jp/kegg/) enriched putative pathways for 52 differentially expressed proteins by RPPA. Data are expressed as number of cleaved caspase-3-positive cells per high-power field. Experiments were repeated in triplicate. Data are presented as mean ± standard deviation (SD). Differences between treatment groups were determined by orthogonal contrasts and denoted as follows: *$p < 0.05$, **$p < 0.01$, ***$p < 0.001$; *ns*, no significance.

diseases (EGFR tyrosine kinase inhibitor resistance and endocrine resistance), and one in cellular processes (P53 signaling pathway). Among these, the Hippo signaling pathway, which has been reported to contribute to anoikis evasion (Zhao et al., 2012), has been identified as a candidate for NE-induced signaling. Its well-known downstream effector YAP1 (Howe and Juliano, 2000; Misra and Irvine, 2018) and upstream regulator NF2 (Reginensi et al., 2016) were both indicated in the enriched KEGG network (Figure 2D).

Our reverse phase protein array data indicated that phosphorylation level of YAP1^{S127} and total NF2 protein were significantly decreased by 82.60% and 90.42%, respectively, in NE-treated SiHa cells (Figures 1E and 1F). Consistent with this finding, when CaSki and ME-180 cells were exposed to 10 μM NE under both normal and low-attachment conditions, phosphorylated YAP1^{S127} and NF2 were significantly downregulated in CaSki and ME-180 cells ($p < 0.01$; Figures 3A and 3B) but not in C33A cells (ADRB2-negative; $p > 0.05$; Figure 3C).

YAP1 Activation Is Required for NE-Induced Anoikis Resistance

Phosphorylation of YAP1^{S127} generates a 14-3-3-binding motif responsible for YAP1 cytoplasmic retention (Zhao et al., 2007); if dephosphorylated, activated YAP1 can translocate into the nucleus and promote transcription of genes that in turn inhibit apoptosis (Kapoor et al., 2014; Yu and Guan, 2013; Yu et al., 2012a). We used immunofluorescence to visualize the intracellular localization of YAP1 in CaSki and ME-180 cells treated with or without 10 μM NE for 2 h and found a clear shift in YAP1 expression from the cytoplasm to the nucleus after NE treatment (Figures 4A and 4B). Consistently, nuclear YAP1 protein expression was significantly higher in mice exposed to restraint stress than those without restraint stress, and propranolol treatment completely abrogated this effect (Figures 4C and 4D). To determine whether similar findings are noted in human samples, we obtained cervical cancer samples from eleven patients. Levels of depressive scores were measured during the pre-surgical clinic visit 1 to 7 days prior to tumor resection. Based on the established threshold of CESD ≥ 16, six participants were determined to have high levels of biobehavioral risk factors, whereas five were low risk. Nuclear staining of YAP1 was significantly higher in patients with cervical cancer with high CESD scores than those without ($p < 0.05$; Figures 4E and 4F).

Next, we used two siRNAs to knock down YAP1 gene expression in CaSki cells ($p < 0.01$ and $p < 0.05$; respectively; Figure 4G) and ME-180 cells ($p < 0.05$ and $p < 0.01$, respectively; Figure 4H). NE 10 μM for 72 h inhibited anoikis in cervical cancer cells transfected with control siRNAs, whereas YAP1 siRNAs abrogated this NE-induced anoikis resistance in both CaSki (Figure 4I) and ME-180 (Figure 4J) cells under anchorage-independent conditions. In addition, when expression of NF2 was downregulated by two siRNAs (Figures S4A and S4B), phosphorylated YAP1^{S127} was decreased (Figures S4C and S4D), and NE-induced anoikis resistance was completely reversed ($p < 0.05$; Figures S4E and S4F).

NE Regulates Hippo-YAP1 Pathway via ADRB2-Mediated Signaling

We next delineated the signaling pathway involved in NE-mediated Hippo-YAP1 activation. Following NE treatment for 1–3 h, in addition to expression changes in NF2 and pYAP1^{S127}, two core kinases in the Hippo pathway, mammalian Ste20-like kinase 1 (MST1) and large tumor suppressor kinase 1 (LATS1), were both dephosphorylated and inactivated (Figure 5A). When cells were pretreated with 10 μM propranolol, 10 μM atenolol (ADRB1 antagonist), or 10 μM ICI-118,551 (ADRB2 antagonist) for 1 h before NE exposure, NE-induced anoikis resistance was abrogated completely by propranolol and ICI-118,551 (Figures 5B and 5C). Furthermore, treatment with ICI-118,551 or propranolol resulted in abrogation of the NE-mediated decrease in YAP1 phosphorylation (Figure 5D); ADRB2 silencing by siRNAs in CaSki and ME-180 cells (Figures S5A and S5B) resulted in abrogation of NE-mediated YAP1 dephosphorylation (Figures S5C–S5E). When ADRB2 was overexpressed using the p6596 ADRB2 plasmid in C33A cells, YAP1 was dephosphorylated by NE (Figure S6).

Because cAMP is an important component of the ADRB2 signaling pathway, we examined intracellular cAMP levels after NE treatment. Relative to controls, treatment with 10 μM NE for 30 min increased cAMP levels by 2.92-fold in CaSki ($p < 0.05$), 3.32-fold in SiHa ($p < 0.05$), and 3.97-fold in ME-180 ($p < 0.05$) cells, but no change was noted in C33A cells ($p > 0.05$) (ADRB2-negative; Figure 6A). Treatment with 10 μM forskolin (cAMP activator) induced similar anoikis resistance in CaSki ($p < 0.05$) and ME-180 ($p < 0.05$) cells (Figure 6B). Exposure to 10 μM forskolin for various durations decreased pYAP1^{S127} expression, much like NE treatment did (Figure 6C). Protein kinase A (PKA) is an important protein downstream of

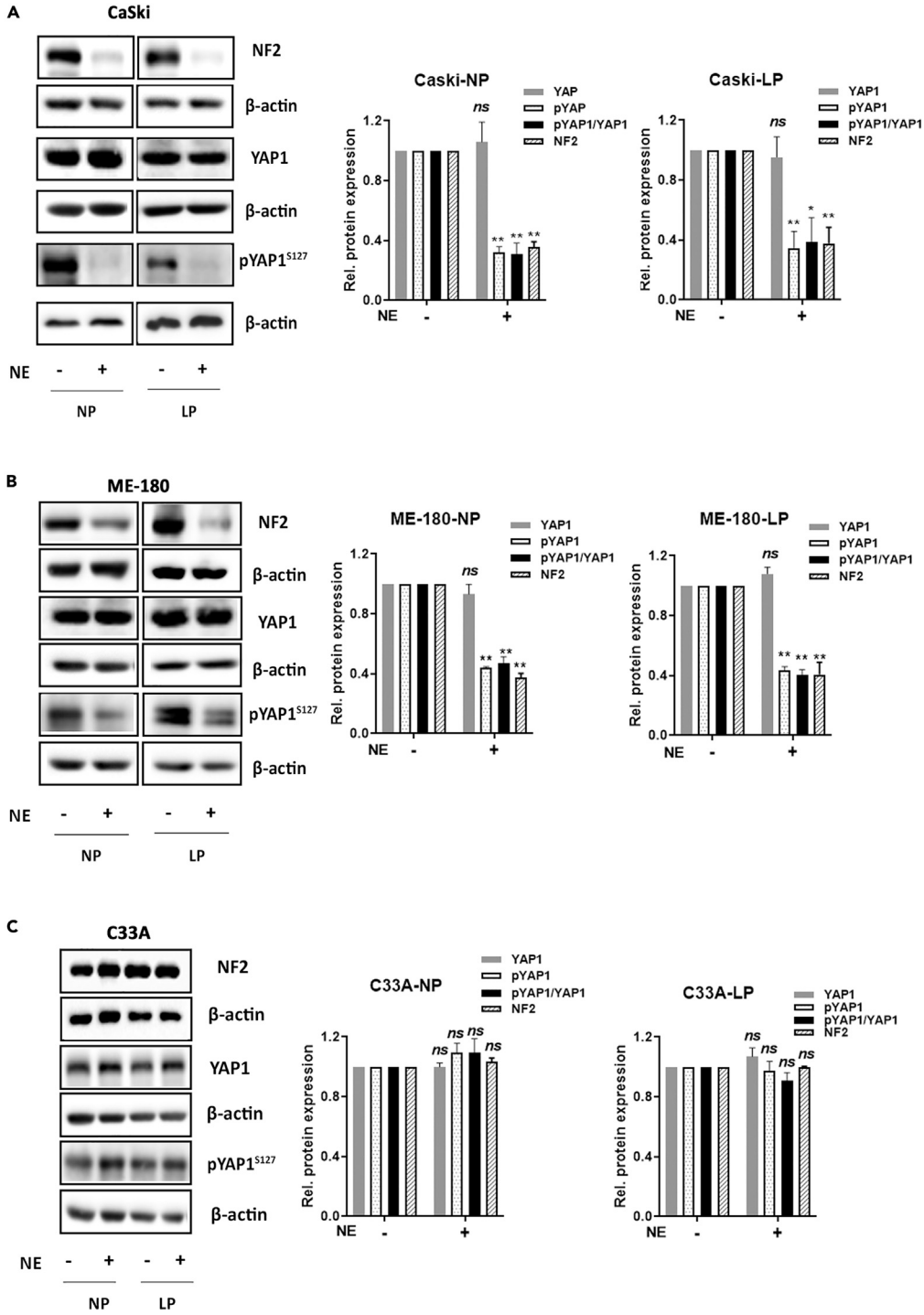

Figure 3. NE Decreases YAP1 Phosphorylation and NF2 Expression in CaSki and ME-180 Cells

Western blot analysis of phosphorylated YAP1^{S127}, total YAP1, and NF2 in CaSki (A), ME-180 (B), and C33A (C) cultured in normal plates (NP) or ultra-low attachment plates (LP) with or without 10 μM NE co-incubation. β-Actin was used as a loading control. The immunoblots are on the left, and quantifications of band intensity relative to β-actin are on the right (n = 3, data represent the mean ± SD). Differences between treatment groups were determined by orthogonal contrasts and denoted as follows: *p < 0.05, **p < 0.01; *ns*, no significance.

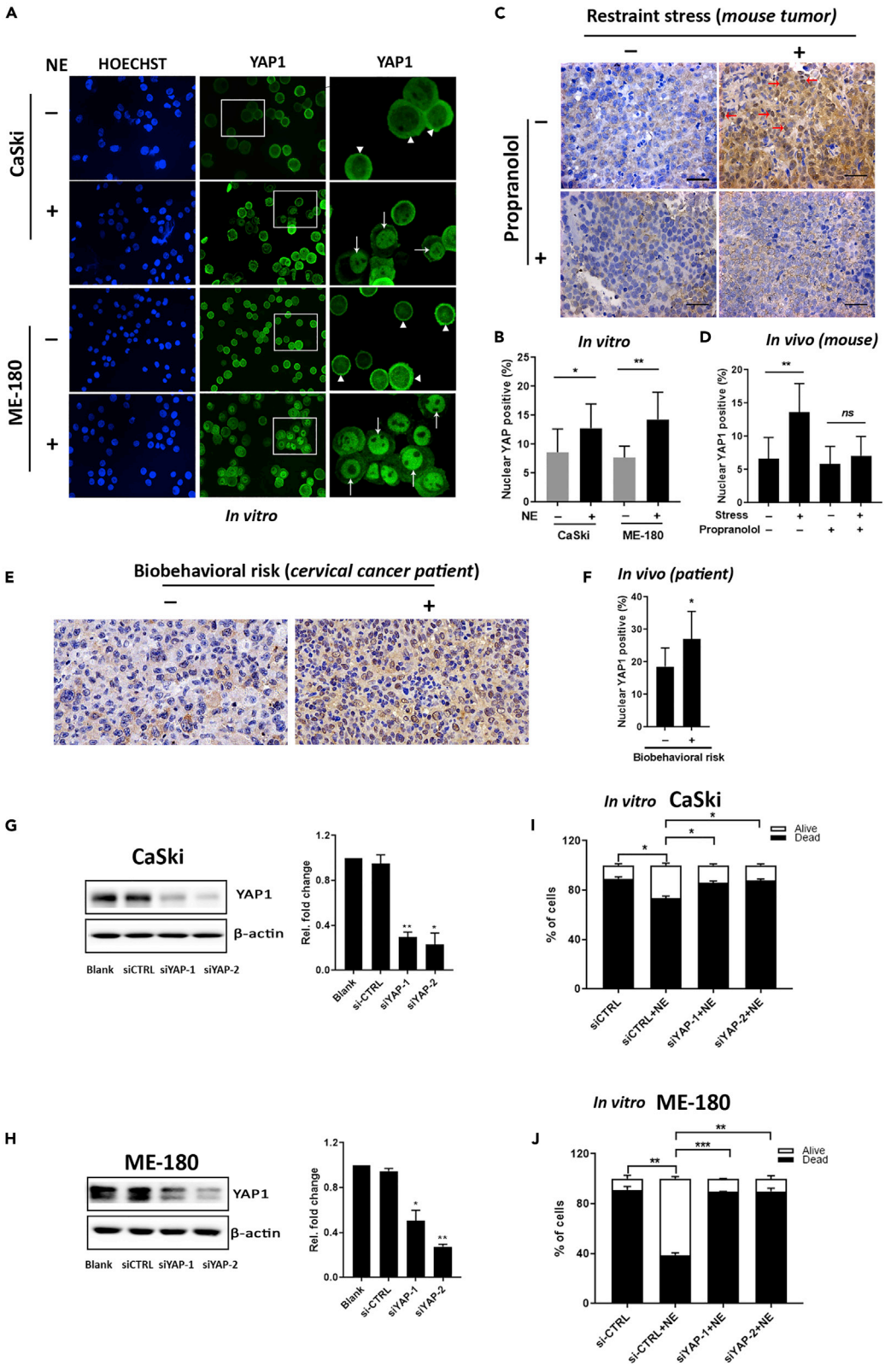
A
NE
HOECHST
YAP1
YAP1
CaSki
ME-180
In vitro
C
Restraint stress (mouse tumor)
Propranolol
B
In vitro
Nuclear YAP positive (%)
NE
CaSki
ME-180
D
In vivo (mouse)
Nuclear YAP1 positive (%)
ns
Stress
Propranolol
E
Biobehavioral risk (cervical cancer patient)
F
In vivo (patient)
Nuclear YAP1 positive (%)
Biobehavioral risk
G
CaSki
YAP1
β-actin
Blank siCTRL siYAP-1 siYAP-2
Rel. fold change
Blank
si-CTRL
siYAP-1
siYAP-2
I
In vitro CaSki
Alive
Dead
% of cells
siCTRL
siCTRL+NE
siYAP-1+NE
siYAP-2+NE
H
ME-180
YAP1
β-actin
Blank siCTRL siYAP-1 siYAP-2
Rel. fold change
Blank
si-CTRL
siYAP-1
siYAP-2
J
In vitro ME-180
Alive
Dead
% of cells
si-CTRL
si-CTRL+NE
siYAP-1+NE
siYAP-2+NE

Figure 4. YAP1 Is Activated by NE and Is Indispensable for NE-Induced Anoikis Resistance

(A–J) (A) Representative immunofluorescence staining and (B) quantification of YAP1 in CaSki and ME-180 cells after 2 h under low-attachment conditions with (bottom) or without (top) 10 μM NE treatment. Representative immunohistochemical staining and quantification of YAP1 in cervical cancer tissues from orthotopic mice (C and D, n = 6) and patients (E and F) (×400 magnification). Western blot analysis (G, left part) in CaSki and ME-180 (H, left part) cells showing knockdown efficiency of YAP1 at the protein level using two siRNAs. (Right part of G and H) Quantifications of band intensity relative to β-actin. Bar graphs showing number of dead (STYOX Red-positive, black) and living (SYTOX Red-negative, white) CaSki (I) and ME-180 (J) cells after 72 h of low attachment. Bars and error bars represent mean ± SD.*$p < 0.05$, **$p < 0.01$ and ***$p < 0.001$. CTRL, control. Arrow：YAP1 expression in the nucleus；arrow head: YAP1 expression in the cytoplasm.

cAMP, and inhibition of PKA (using 10 μM H-89) markedly protected against NE-induced anoikis resistance (Figures 6D and 6E).

DISCUSSION

The key finding of this study is that chronic stress protects cervical cancer cells from anoikis and this protection promotes malignant tumor progression. Here, we developed a preclinical orthotopic mouse model of cervical cancer to provide a new understanding of the effects of chronic stress on cervical cancer growth and metastasis. HPV-16 is the most common HPV genotype in cervical cancer; ME-180 cells are HPV-68 positive; the oncogenic ability is lower than HPV-16, so ME-180 was not selected for orthotopic model. Even though Caski cell and SiHa cells both are HPV-16 positive, we found that CaSki did not have orthotopic tumorigenic potential in the mouse cervix, partially attributed to the fact that CaSki cells are derived from a metastatic site (small intestine). Thus, SiHa cells (HPV16 positive) were used for the orthotopic mouse model. Our data obtained using this model indicate that the neuroendocrine stress response by NE directly induces anoikis resistance through a signaling pathway mediated by Hippo-YAP1 that is initiated by ADRB2/cAMP/PKA activation. Anoikis is a process by which normal cells undergo apoptosis when detached from the surrounding extracellular matrix. Avoidance of anoikis is an essential prerequisite for tumor metastasis; it provides a selective advantage that allows metastatic cancer cells to transit to new sites for attachment (Frisch and Screaton, 2001). Previously, we demonstrated an important role for YAP1 signaling in blocking anoikis (Haemmerle et al., 2017). Similarly, other groups have demonstrated Hippo pathway-mediated anoikis inhibition in hepatocellular carcinoma (Cheng et al., 2018); YAP/TAZ activation by ASPP1 leads to anoikis resistance (Vigneron et al., 2010). In the present study, we implicate sustained adrenergic stimulation in inducing cervical cancer anoikis resistance by inhibition of the tumor suppressive Hippo-YAP1 pathway.

The Hippo-YAP1 pathway plays an important role in regulating cell proliferation, death, and differentiation (Yu and Guan, 2013). The tight control of this pathway and its cross talk with other signaling pathways is critical for tumorigenesis and cancer progression (Yu et al., 2013). Several modulators of the Hippo-YAP1/TAZ pathway have been identified via extensive genetic and biochemical analyses (Yu and Guan, 2013; Zhao et al., 2010, 2011); the Hippo-YAP1/TAZ pathway is robustly regulated by a wide range of signals and their corresponding G protein-coupled receptors (Yu et al., 2012b). Here, we found that ADRB2, a classic G protein-coupled receptor, mediates NE-induced YAP1 activation in cervical carcinogenesis, which indicates that neuroendocrine stress signaling takes part in non-canonical regulation of the Hippo-YAP1 pathway.

Activation of ADRB2 by epinephrine, NE, or specific agonists typically results in Gs-dependent activation of adenylate cyclase and a subsequent increase in intracellular cAMP (Tan et al., 2007). This increase in cAMP stimulates PKA to phosphorylate multiple target proteins, including transcription factors of the CREB/ATF and GATA families (Cole and Sood, 2012; Rockman et al., 2002). Similarly, we found that intracellular cAMP levels in cervical cancer cells were increased by NE stimulation and NE-induced effects could be mimicked by cAMP activation and blocked by a PKA antagonist. Neurofibromin 2 (NF2, also known as merlin), a tumor suppressor and an upstream component of the Hippo pathway, is a direct target of PKA (Alfthan et al., 2004). Our study identified a new functional role for NF2 as a key molecular effector that links adrenergic signaling to the downstream Hippo-YAP1 pathway and tumor progression.

Considering the role of stress-induced suppression of protective immune responses in infection-related cancer (Antoni and Dhabhar, 2019), HPV-driven cervical cancer is potentially much more sensitive to effects of chronic stress than other cancers. Lu et al. found that major life events, including bereavement, severe illness of a family member, divorce, and being between jobs, were prevalent among patients with cervical cancer (37.4%) (Lu et al., 2019). We previously reported that intra-tumoral NE levels in primary ovarian carcinomas are linked to both disease severity and patient psychosocial characteristics (Lutgendorf et al., 2009),

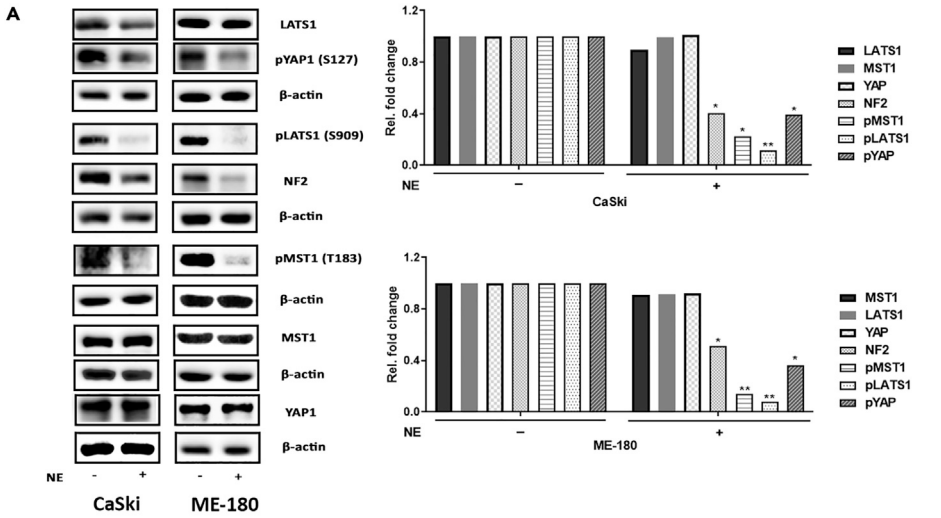
A
LATS1
pYAP1 (S127)
β-actin
pLATS1 (S909)
NF2
β-actin
pMST1 (T183)
β-actin
MST1
β-actin
YAP1
β-actin
NE
CaSki
ME-180
Rel. fold change
LATS1
MST1
YAP
NF2
pMST1
pLATS1
pYAP
CaSki
ME-180

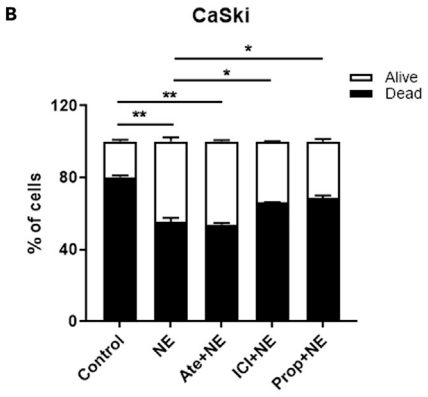
B
CaSki
Alive
Dead
% of cells
Control
NE
Ate+NE
ICI+NE
Prop+NE

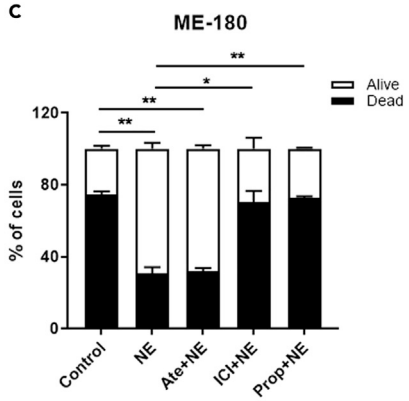
C
ME-180
Alive
Dead
% of cells
Control
NE
Ate+NE
ICI+NE
Prop+NE

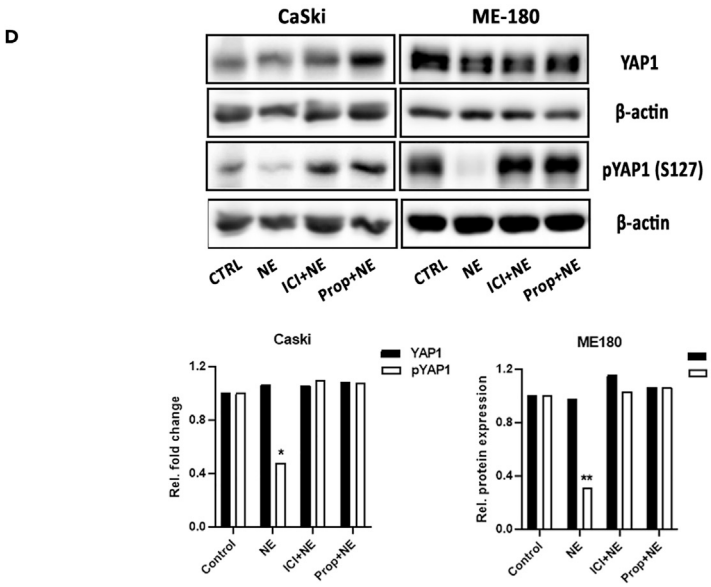
D
CaSki
ME-180
YAP1
β-actin
pYAP1 (S127)
β-actin
CTRL
NE
ICI+NE
Prop+NE
Caski
ME180
YAP1
pYAP1
Rel. fold change
Rel. protein expression
Control
NE
ICI+NE
Prop+NE

Figure 5. NE Regulates Hippo-YAP1 Pathway in CaSki and ME-180 Cells

(A–C) (A) Western blot analysis of YAP1, NF2, and two core kinases in the Hippo pathway were analyzed in CaSki and ME-180 cells with or without 10 μM NE co-incubation. β-Actin was used as a loading control. The immunoblots are on the left, and quantifications of band intensity relative to β-actin are on the right. Effects of atenolol (Ate; ADRB1 antagonist), ICI-118,551 (ICI; ADRB2 antagonist), or propranolol (Prop; non-specific ADRB antagonist) on anoikis in CaSki (B) and ME-180 (C) cells treated with 10 μM NE for 72 h.

(D) Effects of ICI-118,551 or propranolol on phosphorylated $YAP1^{S127}$ and total YAP1 in CaSki and ME-180 cells treated with 10 μM NE for 3 h. The immunoblot is at the top, and quantification of band intensity relative to β-actin is below. Data represent the mean ± SD. *$p < 0.05$, and **$p < 0.01$. CTRL, control.

but very little data about NE levels and β-adrenergic signaling in cervical cancer have been reported to date. In our study, chronic stress induced YAP1 nuclear translocation and anoikis resistance in cervical cancer, and these effects were attenuated by propranolol. These data indicate that pharmacologic inhibition of adrenergic receptors may have therapeutic relevance in cervical cancer. Emerging clinical data also link the use of non-selective β-adrenergic receptor blockers with reduced cancer progression (Barron et al., 2011; De Giorgi et al., 2011; Melhem-Bertrandt et al., 2011). Of note, results of retrospective studies are prone to immortal time bias and need to be further validated in prospective studies (Weberpals et al., 2016).

In summary, our data represent a new understanding of YAP1 activation in response to sustained adrenergic signaling in cervical cancer models (Figure 7). Protective interventions targeting the neuroendocrine system may provide a biologically plausible method to prevent cervical cancer progression.

Limitations of the Study

Although our results demonstrate that norepinephrine induces anoikis resistance in cervical cancer, it is possible that other pathways (e.g., cortisol) could have similar or broader effects. To what extent these stress-related hormones are important in clinical context would require further work. Moreover, in the absence of available syngeneic mouse models, we used cross-species cell line-derived tumor xenograft (CDX) mouse models in this study to understand the role of stress in mediating cancer cell-driven mechanisms of cervical cancer progression. However, it is possible that the tumor microenvironment may also play an important role; immune-competent models would be required for such work.

Resource Availability

Lead Contact

Anil K. Sood, MD Department of Gynecologic Oncology and Reproductive Medicine, The University of Texas MD Anderson Cancer Center, 1155 Herman Pressler, Houston, TX 77030, Tel 713-745-5266, Fax 713-792-7586 (Email: asood@mdanderson.org).

Materials Availability

No new materials were generated in this study.

Data and Code Availability

The raw data that support the findings of this study are available from the corresponding authors, upon request.

METHODS

All methods can be found in the accompanying Transparent Methods supplemental file.

SUPPLEMENTAL INFORMATION

Supplemental Information can be found online at https://doi.org/10.1016/j.isci.2020.101289.

ACKNOWLEDGMENTS

The authors thank Dr. Jing Xu at Fudan University who recruited patients and collected samples for this study. We also acknowledge support from the Foundation for Women's Cancer, Zhejiang Natural Science Foundation (LY19H160038), Talent Project of Zhejiang Association for Science and Technology (2017YCGC001), China Scholarship Council, the core grant P30CA016672 from MD Anderson, the American Cancer Society Research Professor Award, ME STRONG (a 501c# charity), and the Frank McGraw Memorial Chair in Cancer Research. This work was also supported by funds from the MD Anderson Cancer

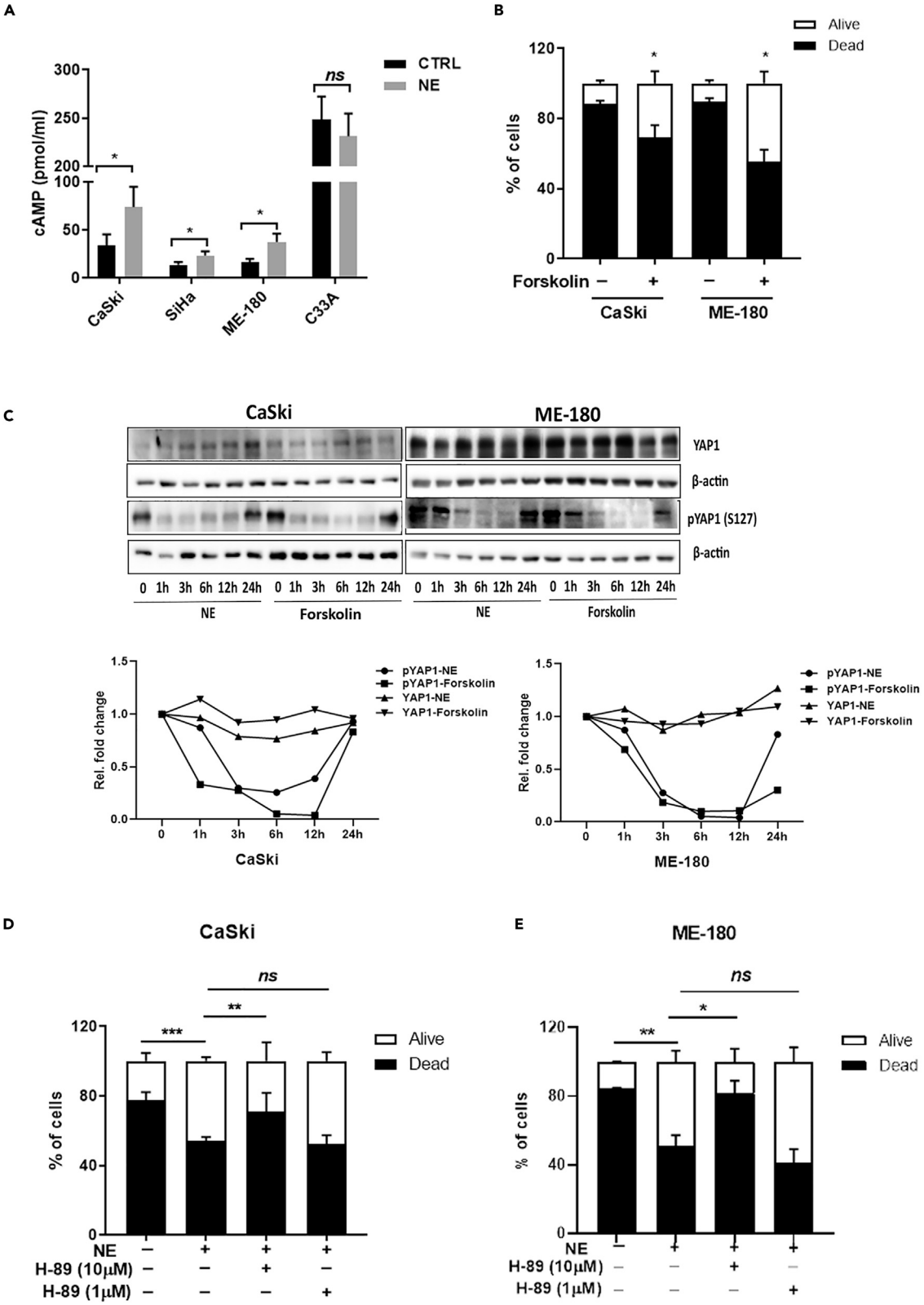
A
cAMP (pmol/ml)
300
250
200
100
50
0
CTRL
NE
ns
*
CaSki
SiHa
ME-180
C33A
B
Alive
Dead
% of cells
120
80
40
0
Forskolin – + – +
CaSki
ME-180
C
CaSki
ME-180
YAP1
β-actin
pYAP1 (S127)
β-actin
0 1h 3h 6h 12h 24h 0 1h 3h 6h 12h 24h 0 1h 3h 6h 12h 24h 0 1h 3h 6h 12h 24h
NE
Forskolin
NE
Forskolin
Rel. fold change
1.5
1.0
0.5
0.0
pYAP1-NE
pYAP1-Forskolin
YAP1-NE
YAP1-Forskolin
0 1h 3h 6h 12h 24h
CaSki
ME-180
D
CaSki
ns
**
***
Alive
Dead
% of cells
120
80
40
0
NE – + + +
H-89 (10μM) – – + –
H-89 (1μM) – – – +
E
ME-180
ns
*
**
Alive
Dead
% of cells
120
80
40
0
NE – + + +
H-89 (10μM) – – + –
H-89 (1μM) – – – +

Figure 6. cAMP and Protein Kinase A (PKA) Mediate NE-Induced Anoikis Resistance and YAP1 Activation

(A) Baseline and NE-induced levels of intracellular cyclic adenosine monophosphate (cAMP) in cervical cancer cells measured by enzyme-linked immunosorbent assay (n = 3).

(B) Effects of 10 μM forskolin (cAMP activator) on anoikis in CaSki and ME-180 cells.

(C–E) (C) Expression pattern of $pYAP1^{S127}$ and total YAP1 at different time points on western blot analysis (n = 2). The immunoblot is at the top, and quantification of band intensity relative to β-actin is below. Effect of H-89 (PKA antagonist, 10 μM or 1 μM incubated for 1 h before NE exposure) on anoikis in CaSki (D) and ME-180 (E) cells.

*p < 0.05; **p < 0.01; ***p < 0.001; *ns*, no significance.

Fund and the Harbin Medical University Cancer Hospital Fund via the Sister Institution Network Fund at the University of Texas MD Anderson Cancer Center. We also thank Dr. Sarah Bronson from the Department of Scientific Publications for reviewing and editing our manuscript.

AUTHOR CONTRIBUTIONS

Conceptualization, Y.L., S.Y., and A.K.S; Methodology, Y.L., N.C.S., L.W., Y.K., L.S.M., Y.S.; Investigation, Y.L., S.Y., S.Z., C.L. and K.L.; Writing – Original Draft, Y.L. and S.Y.; Writing –Review & Editing, Y.L., W.H., L.M.R., Y.L., S.W.C., S.K.L., S.K.D., and A.K.S.; Funding Acquisition, Y.L., S.Y., W.H., and A.K.S.; Supervision, A.K.S.

DECLARATION OF INTERESTS

A.K.S.: Consulting (Merck, Kiyatec), shareholder (BioPath), research funding (M-Trap).

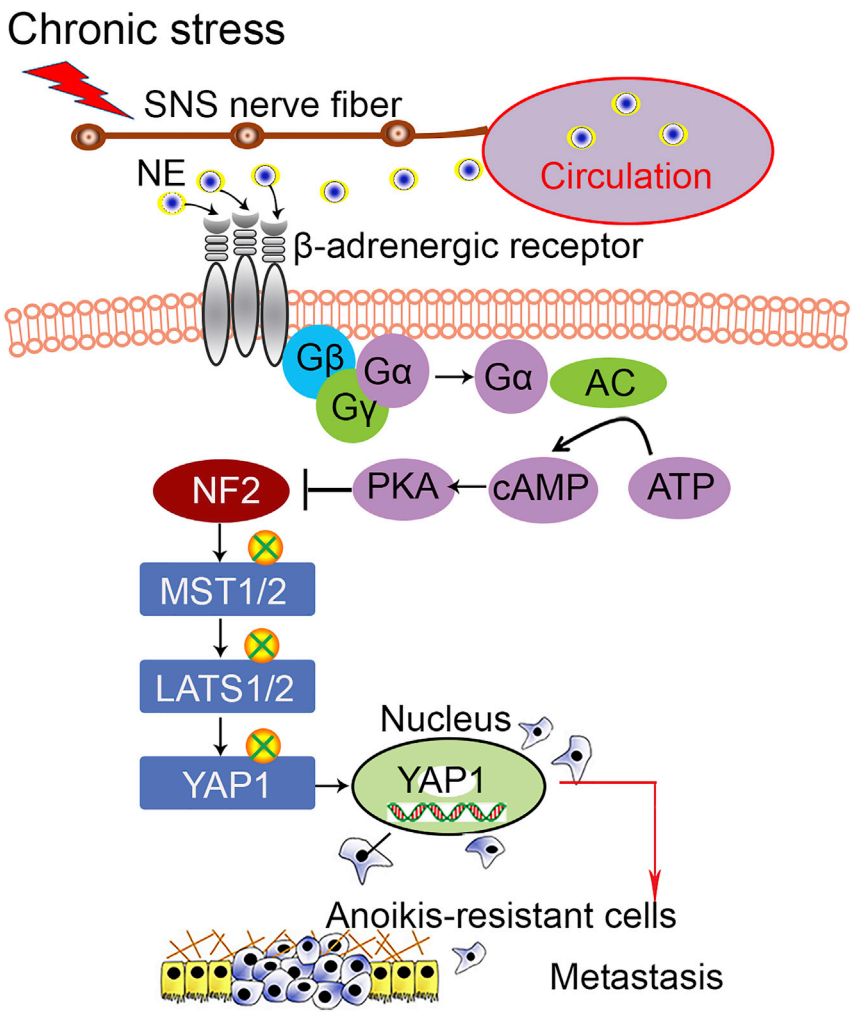

Figure 7. Working Model of NE-Induced YAP1 Activation and Anoikis Resistance in Cervical Cancer Cells

CellPress
OPEN ACCESS

Received: October 6, 2019
Revised: April 19, 2020
Accepted: June 15, 2020
Published: July 24, 2020

REFERENCES

Alfthan, K., Heiska, L., Gronholm, M., Renkema, G.H., and Carpen, O. (2004). Cyclic AMP-dependent protein kinase phosphorylates merlin at serine 518 independently of p21-activated kinase and promotes merlin-ezrin heterodimerization. J. Biol. Chem. *279*, 18559–18566.

Antoni, M.H., and Dhabhar, F.S. (2019). The impact of psychosocial stress and stress management on immune responses in patients with cancer. Cancer *125*, 1417–1431.

Antoni, M.H., Lutgendorf, S.K., Cole, S.W., Dhabhar, F.S., Sephton, S.E., McDonald, P.G., Stefanek, M., and Sood, A.K. (2006). The influence of bio-behavioural factors on tumour biology: pathways and mechanisms. Nat. Rev. Cancer *6*, 240–248.

Barron, T.I., Connolly, R.M., Sharp, L., Bennett, K., and Visvanathan, K. (2011). Beta blockers and breast cancer mortality: a population- based study. J. Clin. Oncol. *29*, 2635–2644.

Bray, F., Ferlay, J., Soerjomataram, I., Siegel, R.L., Torre, L.A., and Jemal, A. (2018). Global cancer statistics 2018: GLOBOCAN estimates of incidence and mortality worldwide for 36 cancers in 185 countries. CA Cancer J. Clin. *68*, 394–424.

Burd, E.M. (2003). Human papillomavirus and cervical cancer. Clin. Microbiol. Rev. *16*, 1–17.

Cheng, Y., Hou, T., Ping, J., Chen, T., and Yin, B. (2018). LMO3 promotes hepatocellular carcinoma invasion, metastasis and anoikis inhibition by directly interacting with LATS1 and suppressing Hippo signaling. J. Exp. Clin. Cancer Res. *37*, 228.

Cole, S.W., Nagaraja, A.S., Lutgendorf, S.K., Green, P.A., and Sood, A.K. (2015). Sympathetic nervous system regulation of the tumour microenvironment. Nat. Rev. Cancer *15*, 563–572.

Cole, S.W., and Sood, A.K. (2012). Molecular pathways: beta-adrenergic signaling in cancer. Clin. Cancer Res. *18*, 1201–1206.

De Giorgi, V., Grazzini, M., Gandini, S., Benemei, S., Lotti, T., Marchionni, N., and Geppetti, P. (2011). Treatment with beta-blockers and reduced disease progression in patients with thick melanoma. Arch. Intern. Med. *171*, 779–781.

Frisch, S.M., and Screaton, R.A. (2001). Anoikis mechanisms. Curr. Opin. Cell Biol. *13*, 555–562.

Haemmerle, M., Taylor, M.L., Gutschner, T., Pradeep, S., Cho, M.S., Sheng, J., Lyons, Y.M., Nagaraja, A.S., Dood, R.L., Wen, Y., et al. (2017). Platelets reduce anoikis and promote metastasis by activating YAP1 signaling. Nat. Commun. *8*, 310.

Howe, A.K., and Juliano, R.L. (2000). Regulation of anchorage-dependent signal transduction by protein kinase A and p21-activated kinase. Nat. Cell Biol. *2*, 593–600.

Kapoor, A., Yao, W., Ying, H., Hua, S., Liewen, A., Wang, Q., Zhong, Y., Wu, C.J., Sadanandam, A., Hu, B., et al. (2014). Yap1 activation enables bypass of oncogenic Kras addiction in pancreatic cancer. Cell *158*, 185–197.

Lu, D., Andrae, B., Valdimarsdottir, U., Sundstrom, K., Fall, K., Sparen, P., and Fang, F. (2019). Psychological distress is associated with cancer-specific mortality among patients with cervical cancer. Cancer Res. https://doi.org/10.1158/0008-5472.CAN-19-0116.

Lu, D., Sundstrom, K., Sparen, P., Fall, K., Sjolander, A., Dillner, J., Helm, N.Y., Adami, H.O., Valdimarsdottir, U., and Fang, F. (2016). Bereavement is associated with an increased risk of HPV infection and cervical cancer: an epidemiological study in Sweden. Cancer Res. *76*, 643–651.

Lutgendorf, S.K., DeGeest, K., Sung, C.Y., Arevalo, J.M., Penedo, F., Lucci, J., 3rd, Goodheart, M., Lubaroff, D., Farley, D.M., Sood, A.K., et al. (2009). Depression, social support, and beta-adrenergic transcription control in human ovarian cancer. Brain Behav. Immun. *23*, 176–183.

Melhem-Bertrandt, A., Chavez-Macgregor, M., Lei, X., Brown, E.N., Lee, R.T., Meric-Bernstam, F., Sood, A.K., Conzen, S.D., Hortobagyi, G.N., and Gonzalez-Angulo, A.M. (2011). Beta-blocker use is associated with improved relapse-free survival in patients with triple-negative breast cancer. J. Clin. Oncol. *29*, 2645–2652.

Misra, J.R., and Irvine, K.D. (2018). The Hippo signaling network and its biological functions. Annu. Rev. Genet. *52*, 65–87.

Reginensi, A., Enderle, L., Gregorieff, A., Johnson, R.L., Wrana, J.L., and McNeill, H. (2016). A critical role for NF2 and the Hippo pathway in branching morphogenesis. Nat. Commun. *7*, 12309.

Rockman, H.A., Koch, W.J., and Lefkowitz, R.J. (2002). Seven-transmembrane-spanning receptors and heart function. Nature *415*, 206–212.

Sood, A.K., and Lutgendorf, S.K. (2011). Stress influences on anoikis. Cancer Prev. Res. (Phila) *4*, 481–485.

Tan, K.S., Nackley, A.G., Satterfield, K., Maixner, W., Diatchenko, L., and Flood, P.M. (2007). beta(2) adrenergic receptor activation stimulates pro-inflammatory cytokine production in macrophages via PKA- and NF-kappa B-independent mechanisms. Cell Signal. *19*, 251–260.

Thaker, P.H., Han, L.Y., Kamat, A.A., Arevalo, J.M., Takahashi, R., Lu, C., Jennings, N.B., Armaiz-Pena, G., Bankson, J.A., Ravoori, M., et al. (2006). Chronic stress promotes tumor growth and angiogenesis in a mouse model of ovarian carcinoma. Nat. Med. *12*, 939–944.

Umamaheswaran, S., Dasari, S.K., Yang, P., Lutgendorf, S.K., and Sood, A.K. (2018). Stress, inflammation, and eicosanoids: an emerging perspective. Cancer Metastasis Rev. *37*, 203–211.

Vigneron, A.M., Ludwig, R.L., and Vousden, K.H. (2010). Cytoplasmic ASPP1 inhibits apoptosis through the control of YAP. Genes Dev. *24*, 2430–2439.

Weberpals, J., Jansen, L., Carr, P.R., Hoffmeister, M., and Brenner, H. (2016). Beta blockers and cancer prognosis - the role of immortal time bias: a systematic review and meta-analysis. Cancer Treat. Rev. *47*, 1–11.

Yu, F.X., and Guan, K.L. (2013). The Hippo pathway: regulators and regulations. Genes Dev. *27*, 355–371.

Yu, F.X., Mo, J.S., and Guan, K.L. (2012a). Upstream regulators of the Hippo pathway. Cell Cycle *11*, 4097–4098.

Yu, F.X., Zhang, Y., Park, H.W., Jewell, J.L., Chen, Q., Deng, Y., Pan, D., Taylor, S.S., Lai, Z.C., and Guan, K.L. (2013). Protein kinase A activates the Hippo pathway to modulate cell proliferation and differentiation. Genes Dev. *27*, 1223–1232.

Yu, F.X., Zhao, B., Panupinthu, N., Jewell, J.L., Lian, I., Wang, L.H., Zhao, J., Yuan, H., Tumaneng, K., Li, H., et al. (2012b). Regulation of the Hippo-YAP pathway by G-protein-coupled receptor signaling. Cell *150*, 780–791.

Zhao, B., Li, L., Lei, Q., and Guan, K.L. (2010). The Hippo-YAP pathway in organ size control and tumorigenesis: an updated version. Genes Dev. *24*, 862–874.

Zhao, B., Li, L., Wang, L., Wang, C.Y., Yu, J., and Guan, K.L. (2012). Cell detachment activates the Hippo pathway via cytoskeleton reorganization to induce anoikis. Genes Dev. *26*, 54–68.

Zhao, B., Tumaneng, K., and Guan, K.L. (2011). The Hippo pathway in organ size control, tissue regeneration and stem cell self-renewal. Nat. Cell Biol. *13*, 877–883.

Zhao, B., Wei, X., Li, W., Udan, R.S., Yang, Q., Kim, J., Xie, J., Ikenoue, T., Yu, J., Li, L., et al. (2007). Inactivation of YAP oncoprotein by the Hippo pathway is involved in cell contact inhibition and tissue growth control. Genes Dev. *21*, 2747–2761.

iScience, Volume *23*

Supplemental Information

Sustained Adrenergic Activation of YAP1 Induces Anoikis Resistance in Cervical Cancer Cells

Yang Li, Shanshan Yang, Nouara C. Sadaoui, Wei Hu, Santosh K. Dasari, Lingegowda S. Mangala, Yunjie Sun, Shuangtao Zhao, Linghua Wang, Yuan Liu, Lois M. Ramondetta, Ke Li, Chong Lu, Yu Kang, Steve W. Cole, Susan K. Lutgendorf, and Anil K. Sood

Supplemental Figures

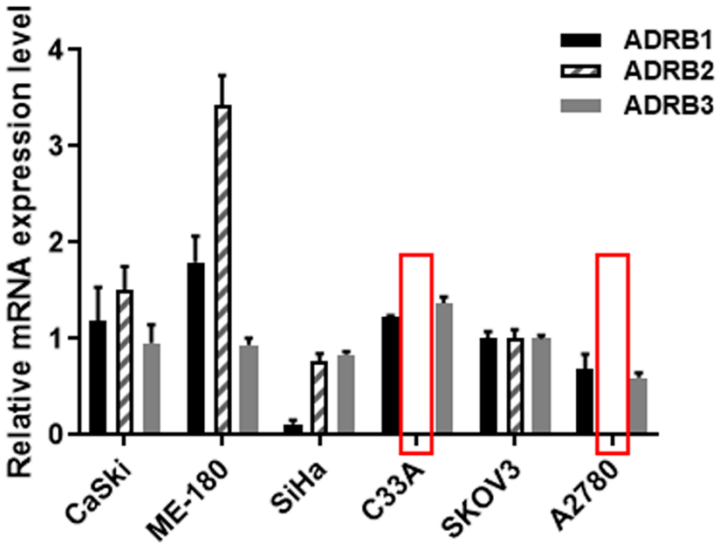

Figure S1. Expression of β-adrenergic receptors ADRB1, ADRB2, and ADRB3 in four cervical and two ovarian cancer cell lines. Red box: Absence of ADRB2 expression. Figure S1. Related to Figure 2.

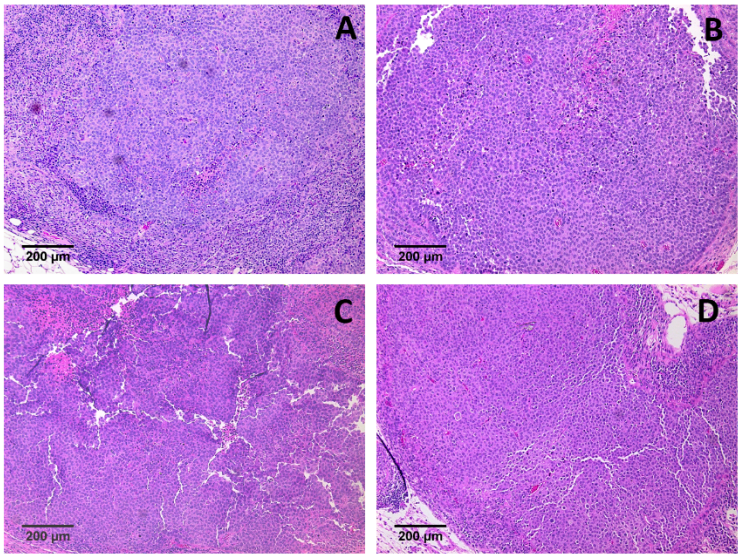

Figure S2. Representative H&E staining of cervical cancer tissues from mice (×100 magnification). Samples were obtained from: (A) control mice without restraint stress; (B) mice exposed to daily restraint stress; (C) mice with propranolol, no restraint stress; (D) mice with propranolol and daily restraint stress. Scale bar is 200 µm**.** Figure S2. Related to Figure 1.

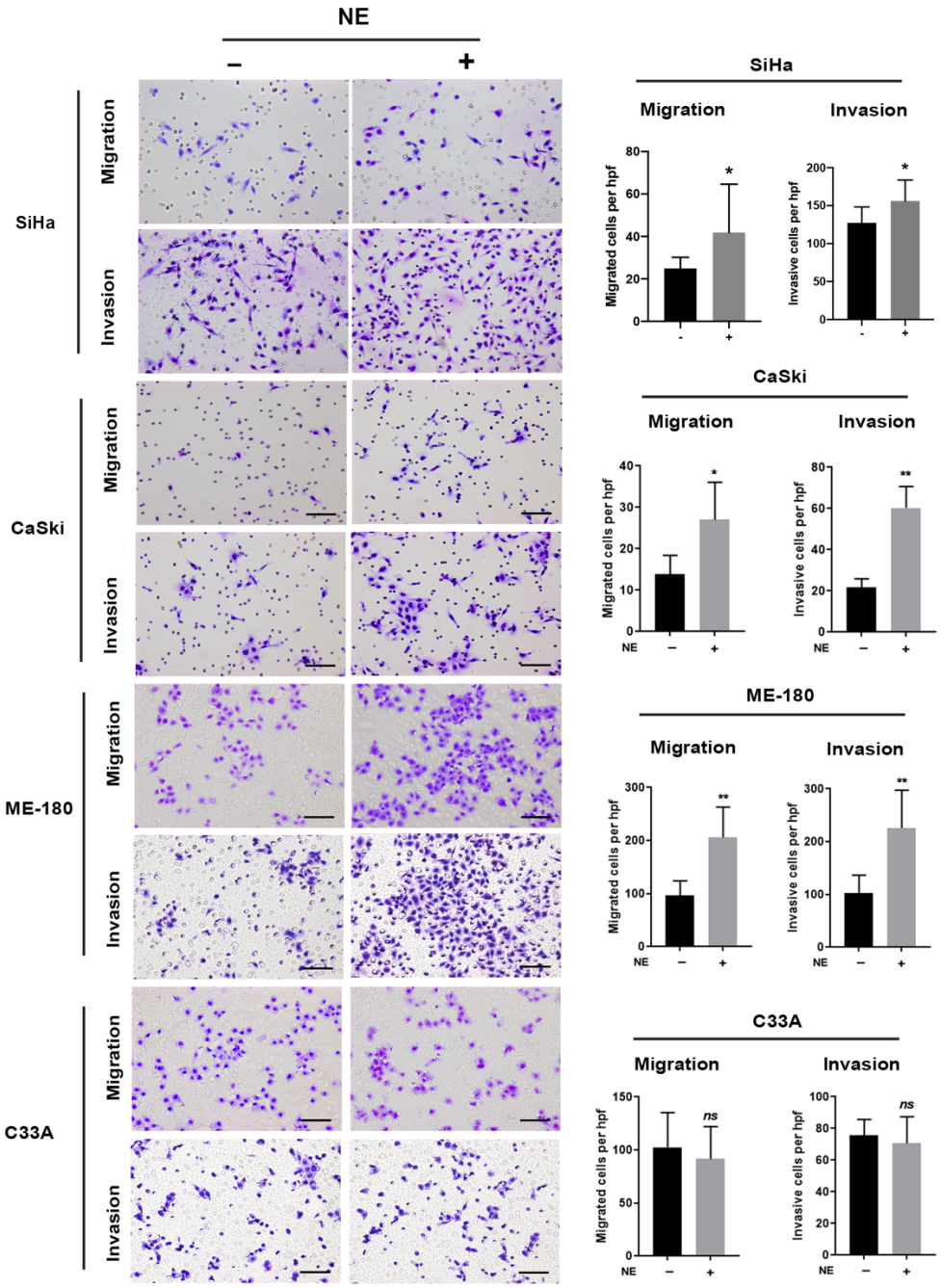

Figure S3. Migration and invasion assay of SiHa, CaSki, ME-180 and C33A cells treated with or without 10 μM NE. Cells per HPF (200×) were counted. Error bars, SD. *P<0.05; **P<0.01; *ns* = no significance. Figure S3. Related to Figure 2.

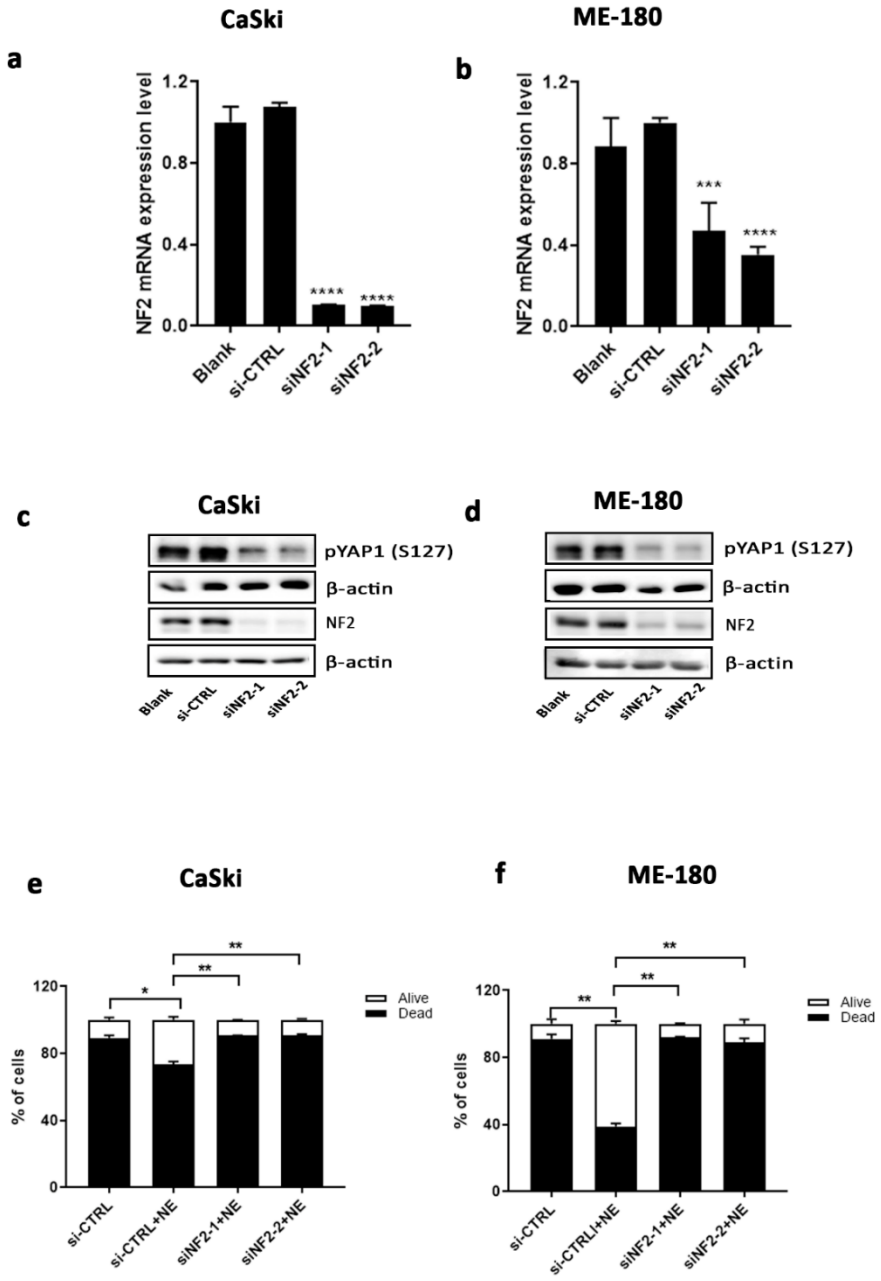

Figure S4. NE-induced anoikis resistance and YAP1 activation are dependent on NF2. Quantitative reverse transcription–polymerase chain reaction (A, B) and Western blot analysis (C, D) in CaSki and ME-180 cells showing efficacy of NF2 knockdown at the RNA and protein levels using two siRNAs. Bar graphs showing number of dead (STYOX Red–positive, black) and living (SYTOX Red–negative, white) CaSki (E) and ME-180 (F) cells after 72 hours of low attachment. Bars and error bars represent mean ± SD. *P<0.05; **P<0.01; ***P<0.001; ****P<0.0001; *ns* = no significance. CTRL: control. Figure S4. Related to Figure 4.

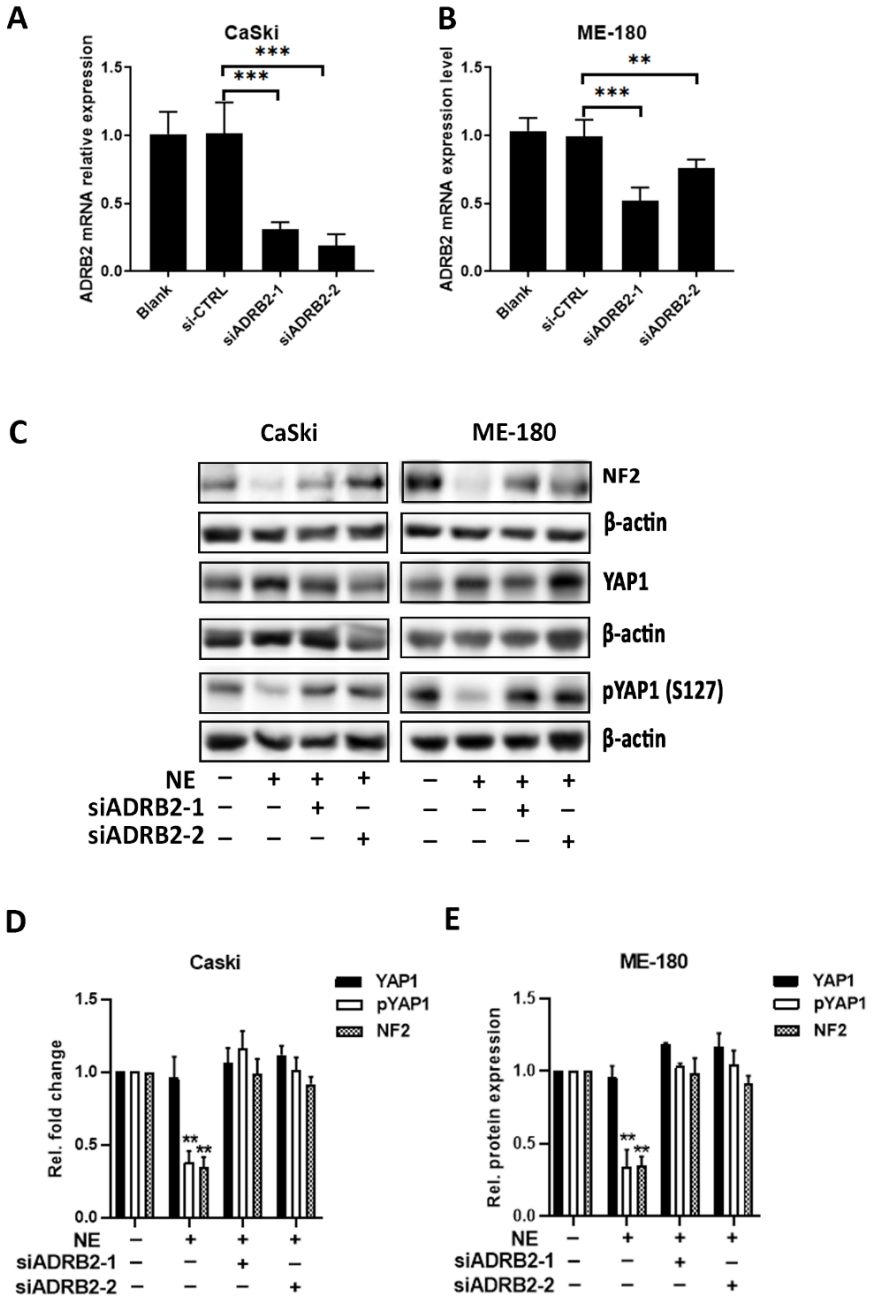

Figure S5. NF2 and YAP1 expression changes after ADRB2 knockdown in CaSki and ME-180 cells. Quantitative reverse transcription–polymerase chain reaction (A, B) in CaSki and ME-180 cells showing efficacy of ADRB2 knockdown at the mRNA level using two siRNAs. (C) Western blot analysis of YAP1 and NF2 expression in CaSki and ME-180 cells transfected with ADRB2 siRNAs. (D, E) Quantification of band intensity relative to β-actin is shown. Data represent the mean ± SD. ***P*<0.01, and ****P*<0.001. CTRL: control. Figure S5. Related to Figure 5.

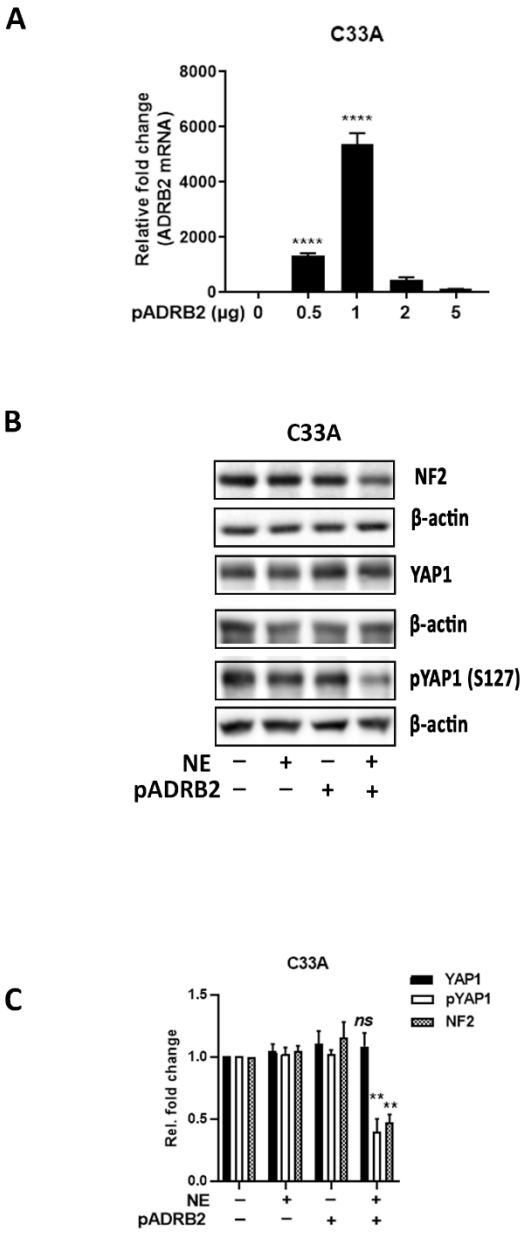

Figure S6. NF2 and YAP1 expression changes after ADRB2 overexpression in C33A cells. Quantitative reverse transcription–polymerase chain reaction (A) in C33A cells showing efficacy of ADRB2 overexpression at the mRNA levels with different amount of plasmid. (B) Western blot analysis of pYAP1, YAP1 and NF2 expression in C33A cells after transfection with ADRB2 plasmid (pADRB2). (C) Quantification of band intensity relative to β-actin is shown. Data represent the mean ± SD. ***P*<0.01, and ****P*<0.001. *ns* = no significance. Figure S6. Related to Figure 5.

Transparent Methods

All experiments were approved and confirmed conform to the relevant regulatory standards of The University of Texas MD Anderson Cancer Center.

STAR Methods

KEY RESOURCES TABLE

REAGENT or RESOURCE	SOURCE	IDENTIFIER
Antibodies		
Anti-YAP1	Cell Signaling Technology	Cat#14074; RRID:AB_2650491
Anti-phospho-YAP (Ser127)	Cell Signaling Technology	Cat# 13008; RRID:AB_2650553
Anti-Phospho-LATS1 (Ser909)	Cell Signaling Technology	Cat# 9157; RRID:AB_2133515
Anti- LATS1	Cell Signaling Technology	Cat# 3477; RRID:AB_2133513
Anti-MST1	Cell Signaling Technology	Cat# 3682; RRID:AB_2144632
Anti-Phospho-MST1 (Thr183)/MST2 (Thr180)	Cell Signaling Technology	Cat# 49332, RRID:AB_2799355
Anti-NF2	Abcam	Cat# ab88957; RRID:AB_2042307
Anti-β-Actin	Sigma-Aldrich	Cat# A5441; RRID:AB_476744
Anti-Cleaved Caspase-3	Cell Signaling Technology	Cat# 9661; RRID:AB_2341188
Alexa Fluor® 488 Goat AntiRabbit IgG	Jackson ImmunoResearch	Cat# 111-546-047; RRID: AB_2338056
ECL™ Anti-Mouse IgG, Horseradish Peroxidase	GE Healthcare	Cat# NA931; RRID:AB_772210
ECL™ Anti-Rabbit IgG, Horseradish Peroxidase	GE Healthcare	Cat# GENA934, RRID: AB_2722659
Chemicals, Peptides, and Recombinant Proteins		
L-(−)-Norepinephrine (+)-bitartrate salt monohydrate	Sigma-Aldrich	Cat# N5785

(±)-Propranolol hydrochloride	Sigma-Aldrich	Cat# P0884
ICI 118,551 hydrochloride	Sigma-Aldrich	Cat# I127
Forskolin	Sigma-Aldrich	Cat# 344270
InSolution H-89, Dihydrochloride	Sigma-Aldrich	Cat# 371962
Atenolol	Tocris	Cat# 0387
Halt Protease Inhibitor Cocktail (100X)	Thermo Fisher Scientific	Cat# 78438
Tris base	Fisher Scientific	Cat# BP152-5
Permount	Fisher Scientific	Cat# SP15-100
Matrigel	BD Biosciences	Cat# 356231
Lipofectamine RNAiMAX transfection reagent	Invitrogen	Cat# 13778500
FuGENE® HD Transfection Reagent	Promega	Cat# E2311
SYTOX® Red Dead Cell Stain	Life technologies	Cat# S34859
Power SYBR® Green PCR Master Mix	Thermo Fisher Scientific	Cat# A25778
Trizol	Invitrogen	Cat# 15596-018
Critical Commercial Assays		
Verso cDNA Synthesis Kit	Thermo Fisher Scientific	Cat# AB1453B
cAMP Parameter Assay Kit	R&B System	Cat# KGE002B
Experimental Models: Cell Lines		
Human: SiHa	ATCC	HTB-35
Human: CaSki	ATCC	CRM-CRL-1550
Human: ME-180	ATCC	HTB-33
Human: C33A	ATCC	HTB-31
Oligonucleotides		
YAP1 siRNA1	Sigma-Aldrich	SASI_Hs01_00182403

YAP1 siRNA2	Sigma-Aldrich	SASI_Hs01_00182404
NF2 siRNA1	Sigma-Aldrich	SASI_Hs01_00188860
NF2 siRNA2	Sigma-Aldrich	SASI_Hs01_00188862
ADRB2 siRNA1	Sigma-Aldrich	SASI_Hs01_00209061
ADRB2 siRNA2	Sigma-Aldrich	SASI_Hs01_00209062
MISSION® siRNA Universal Negative Control #1	Sigma-Aldrich	SIC001
Plasmid		
p6596 MSCV-IP-N-HA ADRB2	Addgene	Plasmid #34895
Software and Algorithms		
Prism Version 8.00	GraphPad	https://www.graphpad.com/
ImageJ	Schneider et al., 2012	https://imagej.nih.gov/ij/
GO	Ashburner, M., et al. 2000	http://geneontology.org/
KEGG	Kanehisa, M et al., 2004	https://www.genome.jp/kegg/

CONTACT FOR REAGENT AND RESOURCE SHARING

Further information and requests for all original resources and reagents presented in this manuscript should be directed and will be fulfilled by the Lead Contact, Anil K Sood (asood@mdanderson.org)

Cell lines and tissue culture

Cervical cancer cell line CaSki was cultured with Roswell Park Memorial Institute (RPMI) 1640 medium, ME-180 was with McCoy's 5A medium, SiHa was with Minimum Essential Medium

(MEM) and C33A was with Dulbecco's Modified Eagle Medium (DMEM); ovarian cancer cell line SKOV3 and A2780 were cultured with RPMI 1640 medium. All cell lines were purchased from the American Type Culture Collection and supplemented with 10% fetal bovine serum (FBS) and 0.1% gentamicin sulfate (Gemini Bio-Products) in 5% CO_2 at 37 °C. All experiments were performed at 70%-80% confluence, and cell lines were routinely screened for mycoplasma.

In vivo model of restraint-stress in an orthotopic model of cervical cancer

All in vivo experiments were approved by the Institutional Animal Care and Use Committee of The University of Texas MD Anderson Cancer Center. 8-12 weeks-old female athymic nude mice were obtained from Taconic Farms. Mice were randomized (10 mice per treatment) into four groups: 1) control with no stress, 2) control with restraint stress, 3) propranolol with no stress, and 4) propranolol with restraint stress. For restraint-stress experiments, nude mice were placed in a movement-restricted space for 2 hours daily as described previously (Thaker et al., 2006). On day 0, mice were underwent a mid-ventral laparotomy, during which they received an injection of 2×10^6 SiHa, CaSki or C33-A cancer cells in 100 µl of Hank's Balanced Salt Solution into the uterine cervix. From day 3, mice were subjected to this movement-restricted stress for 21 days. In the SiHa cervical cancer model, for 21 days, all mice received daily intraperitoneal injection of phosphate-buffered saline (PBS) or propranolol at 2 mg/kg. Seven days after stress was ceased, the mice were sacrificed by cervical dislocation and their tumors were dissected.

Patients and psychological measures

A total of 11 cervical cancer patients who had undergone primary surgical resection at Fudan University, Shanghai between November 2014 and September 2015 were included in this study. All the tumor samples were confirmed to be stage Ib1-IIa squamous cervical carcinomas. This study was approved by the Ethics Committee of the Obstetrics and Gynecology Hospital affiliated to Fudan University. Biobehavioral assessments were carried out using the Center for Epidemiologic Studies Depression Scale (CESD). The CESD is a validated 20-item scale that assesses depressive symptoms occurring in the prior week. Scores of higher than 16 indicate a high biobehavioral risk (Radloff, 1977; Weissman et al., 1977).

siRNA preparation and treatment

Lipofectamine RNAiMAX transfection reagent (Invitrogen) was used according to the manufacturer's protocol to transiently transfect cells. Forward transfection with 40 nM siRNA was performed in cells in normal plates. Media was changed after 6 hours, and cells were collected for RNA or protein extraction at 48 hours after transfection. Cells in suspension, seeded in a low-attachment plate, were transfected with siRNAs (40 nM) by reverse transfection. Antibiotics were added 6 hours later, and NE was added 24 hours later. Cells were cultured for 72 hours for the anoikis assay.

Plasmid transfection

FuGENE HD Transfection Reagent (Promega) was used to transfect p6596 MSCV-IP-N-HA ADRB2 into C33A cells. Media was changed after 6 hours, and cells were collected for RNA or protein extraction at 72 hours after transfection.

Anoikis assay in vitro

Cells (5×10^5 per well) were seeded in an ultra-low attachment six-well plate (#3471, Corning) with incomplete media (no serum). Cells were pretreated with 10 μM PKA inhibitor (H-89), nonselective β-blocker (propranolol), selective ADRB1 antagonist (atenolol), or ADRB2 antagonist (ICI-118,551) for 1 hour and then treated with fresh prepared NE at 10 μM. For Western blot, cells were collected at 1-3 hours. For the anoikis assay, cells were treated with NE or blockers every 12 hours and collected at 72 hours. After incubation, the cells in suspension were harvested and centrifuged at 1500 RPM for 5 minutes. Pellets were washed with cold PBS supplemented with 0.02% FBS twice. Dead cells were quantified by flow cytometry using SYTOX Red Dead Cell Stain (Invitrogen) according to the manufacturer's protocol and then analyzed by flow cytometry using a Beckman Coulter Gallios analyzer.

RNA extraction and quantitative real-time PCR

Total RNA was extracted using a Qiagen RNeasy kit and quantified by spectrophotometry (NanoDrop, Thermo Fisher Scientific). cDNAs were synthesized using the Verso cDNA kit (Thermo Fisher Scientific) according to the manufacturer's instructions. Real-time polymerase chain reaction was performed using a 7500 Fast Real-Time PCR System (Applied Biosystems) with Power SYBR Green PCR Master Mix (Applied Biosystems). 18S was used as a housekeeping gene (RNA18S5, #HP220445, OriGene). The sequences of primers are presented in the Supplementary Table.

Western blotting analysis

Cell lysates were prepared using radioimmunoprecipitation assay buffer (50 mM Tris–HCl [pH 7.4], 150 mM NaCl, 1% Triton, 0.5% deoxycholate) supplemented with Halt Protease and Phosphatase Inhibitor Cocktail (Thermo Fisher Scientific). The protein concentrations were assessed using a BCA Protein Assay reagent kit (Pierce Biotechnology), and proteins were separated via sodium dodecyl sulfate–polyacrylamide gel electrophoresis. Then, proteins were transferred onto a nitrocellulose membrane using electrophoresis (Bio-Rad Laboratories). All membranes were blocked with 5% nonfat dry milk in 1× Tris-buffered saline with Tween 20 for 1 hour and then incubated at 4 °C overnight with the primary antibodies: After washing with 1× Tris-buffered saline with Tween 20, membranes were then incubated with horseradish peroxidase–conjugated anti-mouse or anti-rabbit immunoglobulin G (1:2000; GE Healthcare Life Sciences) for 1 hour at room temperature and exposed using an enhanced ECL Western Blotting Substrate (Pierce Biotechnology). β-actin was used as loading control.

Reverse phase protein analysis and enrichment analysis

Protein lysates were isolated from cells as described above. Samples were diluted to 1.5 μg/μl in radioimmunoprecipitation assay buffer, denatured by 1% sodium dodecyl sulfate with β-mercaptoethanol and stored at −80 °C until further use. Reverse phase protein array was performed at the MD Anderson Functional Proteomics Reverse Phase Protein Array Core facility using 120 μg of protein per sample. All antibodies were validated previously(Tibes et al., 2006). To see associations between the identified gene modules and gene functions, we performed enrichment analyses using GO databases (Biological Process and Molecular Function, http://geneontology.org/) (Ashburner et al., 2000) and KEGG pathways (https://www.genome.jp/kegg/) (Kanehisa et al., 2004). The tools were used with the default options: a significance threshold of 0.05 for adjusted *P* value, at least two genes from the input list in the enriched category, and the whole genome as the reference background.

cAMP quantification

Intracellular levels of cAMP were quantified colorimetrically using a cAMP Parameter Assay Kit (#KGE002B, R&D Systems) according to the manufacturer's instructions. Results are presented as pmol of cAMP per ml of protein.

Immunofluorescence

After culturing in the low attachment plate, the cells were collected and spun down on a coated glass coverslip (#08-774-383, Fisher Scientific), and then fixed in 4% paraformaldehyde for 20 minutes at room temperature, incubated in PBS/0.2% Triton X-100 for 10 minutes and blocked in PBS/10% FBS + 1% bovine serum albumin for 1 hour at room temperature. Thereafter, the fixed cells were incubated at 4 °C overnight with the primary anti-human YAP1 antibody. The next day, Alexa Fluor 488–labeled goat anti-rabbit secondary antibody (1:1000, #ab150077; Abcam) was added for 1 hour at room temperature. Hoechst 33342 (1:10,000, Molecular Probes) was used for nuclear counterstaining. Slides were mounted using ProLong Diamond Antifade Mountant (#P36965, Invitrogen).

Immunohistochemical analysis

Paraffin-embedded tissue slides were deparaffinized, dehydrated, and rehydrated and then processed in a series of xylene and alcohol washes, and antigen retrieval was performed in Diva Decloaker in a pressure cooker. Nonspecific epitopes were blocked in 4% fish gelatin for 1 hour, and the primary antibody, anti–cleaved caspase-3 or YAP1, was incubated overnight at 4 °C. Slides were incubated with horseradish peroxidase–conjugated secondary antibody (Jackson ImmunoResearch) at room temperature for 1.5 hours, and then 3,3′-diaminobenzidine (DAB, Invitrogen) was used to visualize the stains. Next, slides were counterstained with hematoxylin (Invitrogen).

Migration and invasion assays

24–well polycarbonate-membrane modified Boyden chambers (Corning) were used for both assays following previously described protocols (Armaiz-Pena et al., 2013). An 8-μm insert (#141006, Thermo Fisher Scientific) was used for CaSki cells, and a 12-μm Millicell cell insert (PIXP01250) was used for ME-180 and C33A cells. Single-cell suspensions were seeded into the upper wells at a concentration of 1×10^5 cells per well for the invasion assays and 7.5×10^4 cells per well for the migration assays. Cells were incubated at 37 °C in 5% CO_2 for 8-12 hours for migration and 24 hours for invasion. The membranes were fixed, stained, and counted by light microscopy at 200× for quantification.

Statistical analysis

Statistical analysis and data normality test were done using GraphPad Prism 8.0. Differences between two groups were evaluated using a two-tailed Student t-test or one-way analysis of variance. Results are presented as the mean ± standard error of the mean. For all statistical analyses, $P<0.05$ was considered statistically significant.

Supplemental References

Armaiz-Pena, G.N., Allen, J.K., Cruz, A., Stone, R.L., Nick, A.M., Lin, Y.G., Han, L.Y., Mangala, L.S., Villares, G.J., Vivas-Mejia, P.*, et al.* (2013). Src activation by beta-adrenoreceptors is a key switch for tumour metastasis. Nat Commun *4*, 1403.

Ashburner, M., Ball, C.A., Blake, J.A., Botstein, D., Butler, H., Cherry, J.M., Davis, A.P., Dolinski, K., Dwight, S.S., Eppig, J.T.*, et al.* (2000). Gene ontology: tool for the unification of biology. The Gene Ontology Consortium. Nat Genet *25*, 25-29.

Kanehisa, M., Goto, S., Kawashima, S., Okuno, Y., and Hattori, M. (2004). The KEGG resource for deciphering the genome. Nucleic Acids Res *32*, D277-280.

Radloff, L.S. (1977). The CES-D Scale: A Self-Report Depression Scale for Research in the General Population. . Applied Psychological Measurement *1*, 385-401.

Thaker, P.H., Han, L.Y., Kamat, A.A., Arevalo, J.M., Takahashi, R., Lu, C., Jennings, N.B., Armaiz-Pena, G., Bankson, J.A., Ravoori, M.*, et al.* (2006). Chronic stress promotes tumor growth and angiogenesis in a mouse model of ovarian carcinoma. Nat Med *12*, 939-944.

Tibes, R., Qiu, Y., Lu, Y., Hennessy, B., Andreeff, M., Mills, G.B., and Kornblau, S.M. (2006). Reverse phase protein array: validation of a novel proteomic technology and utility for analysis of primary leukemia specimens and hematopoietic stem cells. Mol Cancer Ther *5*, 2512-2521.

Weissman, M.M., Sholomskas, D., Pottenger, M., Prusoff, B.A., and Locke, B.Z. (1977). Assessing depressive symptoms in five psychiatric populations: a validation study. Am J Epidemiol *106*, 203-214.